Bull Math Biol (2014) 76:1783–1808
DOI 10.1007/s11538-014-9977-z

Society for Mathematical Biology

ORIGINAL ARTICLE

# Multiple Surface Reactions in Arrays with Applications to Optical Biosensors

**Matthew E. Zumbrum · David A. Edwards**

Received: 26 November 2013 / Accepted: 9 May 2014 / Published online: 19 July 2014


**Abstract** We analyze surface-volume reactions in the context of optical biosensors with arrays of reacting zones. For arrays having zones with the same rate constants, we consider a two-dimensional reacting zone boundary definition and quantify ligand depletion with the effective Damköhler number. We use asymptotics to obtain ligand depletion results for the one-dimensional case, and also compute results for the circular reacting zone case. For arrays having zones with different rate constants, depletion effects cannot be expressed as the product of time-dependent and space-dependent terms, and we propose two effective rate constant equations for this case.

**Keywords** Surface reactions · Perturbation methods

## List of Symbols

### Variables and Parameters

| | |
|---|---|
| $A$ | Area of reacting zone (17) |
| $a$ | Constant in Da bound |
| $\tilde{B}(\tilde{x}, \tilde{z}, \tilde{t})$ | Bound ligand concentration, units $N/L^2$ |
| $b$ | Constant in Da bound |

If the same letter appears with and without a tilde, the letter with a tilde has dimension and the letter without a tilde is dimensionless. Units are listed in terms of length ($L$), mass ($M$), moles ($N$), or time ($T$).

M. E. Zumbrum (✉)
Department of Mathematics, Temple University, Philadelphia, PA 19122, USA
e-mail: zumbrum@temple.edu

D. A. Edwards
Department of Mathematical Sciences, University of Delaware, Newark, DE 19716, USA
e-mail: edwards@math.udel.edu

| | |
|---|---|
| $\tilde{C}(\tilde{x}, \tilde{y}, \tilde{z}, \tilde{t})$ | Ligand concentration, units $N/L^3$ (1) |
| $\tilde{C}_{\mathrm{u}}$ | Uniform feed ligand concentration, units $N/L^3$ (1) |
| $c$ | Constant in Da bound |
| $\tilde{D}$ | Molecular diffusion coefficient, units $L^2/T$ |
| Da, ${}_i\mathrm{Da}$ | Damköhler number (7) |
| $\mathrm{Da}_i$ | Effective Damköhler number for $i$th reacting zone (18) |
| $d$ | Constant in Da bound |
| $f_1$, $f_2$ | General functions in discussion of the boundedness of $\mathrm{Da}_i(t)$ |
| $g$ | Constant in average ligand depletion |
| $\tilde{H}$ | Height of biosensor channel, units $L$ (1) |
| $H$ | Harmonic number |
| $h$ | Spatial function for ligand concentration (14) |
| $\overline{h}$ | Constant in average ligand concentration |
| $I(x, z)$ | Indicator function for reacting zone (8) |
| $i$ | Row variable |
| $j$ | Column variable |
| $K$ | Scaled affinity constant (5) |
| $\tilde{k}_{\mathrm{on}}$, $\tilde{k}_{\mathrm{off}}$ | Interaction rate constants, units $L^3/NT$ and $1/T$ |
| $\tilde{L}$ | Length of biosensor channel, units $L$ |
| $\tilde{L}_{\mathrm{r}}$ | Diameter of a circular reacting zone, units $L$ (1) |
| $m$ | Parameter for reacting zone boundary definition |
| $n$ | Indexing variable |
| Pe | Peclét number |
| $\tilde{R}$ | Receptor concentration on reacting surface, units $N/L^2$ |
| $\mathcal{R}_{\mathrm{r}}$ | Reacting surface (5) |
| $r$ | Root function (21) |
| $Re$ | Reynolds number |
| $S[\cdot]$ | Sensogram (17) |
| $\tilde{t}$ | Reaction time scale, units $T$ (1) |
| $\tilde{V}$ | Characteristic velocity, units $L/T$ |
| $\tilde{W}$ | Width of biosensor channel, units $L$ |
| $x(z; j)$ | Boundary for reacting zone (21) |
| $\tilde{x}$, $\tilde{y}$, $\tilde{z}$ | Spatial variables, units $L$ (1) |
| $\Gamma$ | Gamma function |
| $\eta$ | Boundary layer variable (2) |
| $\kappa_{\mathrm{on}}$ | Ratio of association rate constant to the first reacting zone association rate constant (28) |
| $\nu$ | Convolution integral variable |

**Other Notation**

| | |
|---|---|
| 0 | as a subscript, used to indicate leading-order perturbation expansion |
| $-$ | as a subscript, used to indicate smaller quadratic root |
| $-$ | as a superscript, used to indicate the beginning of a reacting zone |
| $+$ | as a subscript, used to indicate larger quadratic root |
| $+$ | as a superscript, used to indicate the end of a reacting zone |

## 1 Introduction

Optical biosensors use surface-volume reactions for the measurement of reaction rate constants. Within a biosensor device, a reactant (the receptor) is immobilized on a sensor chip in a region called a reacting zone, and a fluid containing another reactant (the ligand) flows over the reacting zone. Early devices include a single-reacting zone, and mathematical models for this case have been developed (Edwards 1999; Mason et al. 1999; Zumbrum, submitted). Newer technology allows for an array of reacting zones to be included in a single flow channel, allowing for the study of up to 400 reactions simultaneously; an example of this type of flow cell is the Biacore Flexchip (Rich et al. 2008). We display a schematic representation of the Flexchip in Fig. 1. Note that the reacting zones, which are spaced in a rectangular array, are typically circular; our work here is more general, and includes circular zones as a special case. Arrays of reacting zones also arise in biological applications such as multiple-coated pits on cell membranes to which protein ligand binds (Bhattacharyya et al. 2010; Goldstein et al. 1988) and multiple receptor sites on lipid rafts (Pommier et al. 2010).

For each individual reacting zone, biosensors produce a sensogram for the average bound ligand concentration over a reacting zone using a method called surface plasmon resonance (GE Healthcare 2007). Transport effects (most strongly, depletion) have been shown to be important for surface-volume reactions with only a single reacting zone (Edwards 1999; Mason et al. 1999; Zumbrum and Edwards, submitted). The standard model includes a system of partial differential equations (PDE) for the ligand concentration and bound ligand concentration. Due to the high flow rate in the device, the problem may be reduced to a nonlinear ordinary integrodifferential equation for the bound ligand concentration on the reacting surface.

In experimentally realizable regimes, the problem may be simplified further to a simpler nonlinear ordinary differential equation (ODE) using perturbation methods (Edwards 2001; Hansen et al. 2012). This differential equation, called an effective rate constant (ERC) equation, models the average bound ligand concentration over a reacting zone.

Transport effects are complicated further for receptors in several disconnected regions. Motivated by simulations which show that the flow in the Flexchip is nearly

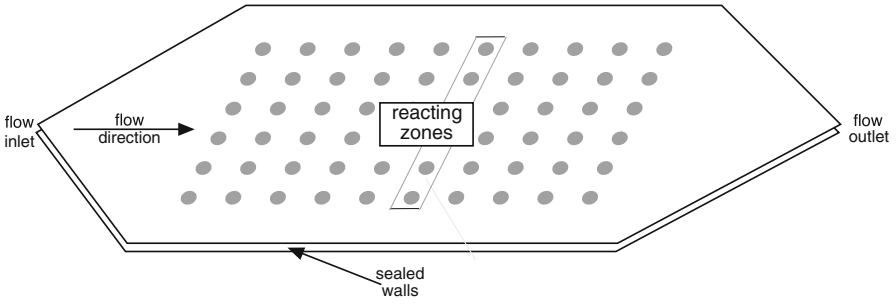


**Fig. 1** Three-dimensional schematic representation of the Flexchip. Note the reacting zones are typically *circles* aligned in a rectangular array

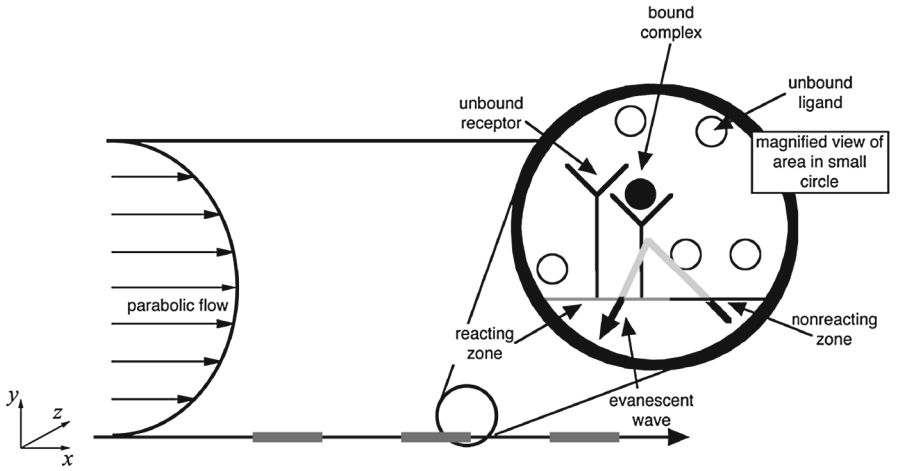


**Fig. 2** Cross-sectional schematic representation of an optical biosensor with three reacting zones

unidirectional (Zumbrum and Edwards, submitted), the Flexchip was first studied using a one-dimensional model, as illustrated in Fig. 2. This is equivalent to considering rectangular zones in a rectangular array; both analytical (Edwards 2011) and numerical (Hu et al. 2007) studies were conducted.

In contrast to those works, in this paper we investigate arrays of two-dimensional reacting zones, as shown in Fig. 3. Our new model, derived in §2 and §3, is general enough to contain both the experimentally realizable circular case and the previously studied rectangular case. We may use similar techniques as in the one-dimensional case, deriving a row-specific ERC equation to account for depletion effects.

Previous one-dimensional models (Edwards 2011; Zumbrum, submitted) considered only the case where the identical receptor is used in each zone. However, arrays of reacting zones are especially useful for quickly analyzing multiple reactions involving the same ligand and different receptors. Thus, in addition to extending the work in Edwards (2011) to the two-dimensional case, we also propose two different ERC equations for arrays of reacting zones with different receptors and discuss the advantages and disadvantages of each in §4.

## 2 Model Background

Biosensor experiments are run in two phases: the injection phase, in which a uniform ligand concentration is fed into the flow channel, and the wash phase, in which no ligand is fed into the channel. For the latter, ligand is only present due to bound receptors. We focus on injection phase dynamics, but results for the wash phase may be obtained similarly. Given the thinness of any three-dimensional reacting zone near the surface, we may treat the reacting zone as a surface (Edwards 1999). Hence, the standard two-compartment model for surface-volume reactions is a convection–diffusion PDE for

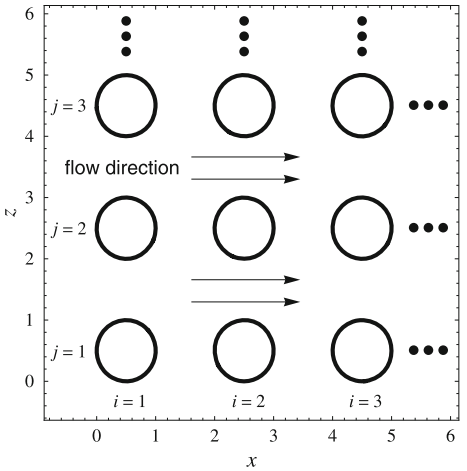


**Fig. 3** Circular reacting zones in rows $i = 1, 2, 3$ and columns $j = 1, 2, 3$

the ligand concentration $\tilde{C}(\tilde{x}, \tilde{y}, \tilde{z}, \tilde{t})$ in the bulk flow coupled to kinetic evolution of the bound ligand concentration $\tilde{B}(\tilde{x}, \tilde{z}, \tilde{t})$ at the reacting surface $\tilde{y} = 0$.

We consider the convection–diffusion equation for ligand concentration, introducing the dimensionless variables

$$x = \frac{\tilde{x}}{\tilde{L}_\mathrm{r}},\ y = \frac{\tilde{y}}{\tilde{H}},\ z = \frac{\tilde{z}}{\tilde{L}_\mathrm{r}},\ \tilde{t} = \frac{1}{\tilde{C}_\mathrm{u}\tilde{k}_\mathrm{on}}t,\ \text{and}\ \tilde{C}(\tilde{x}, \tilde{y}, \tilde{z}, \tilde{t}) = \tilde{C}_\mathrm{u}(1 - \hat{C}(x, y, z, t)), \tag{1}$$

where $\tilde{L}_\mathrm{r}$ is the diameter of a circular reacting zone within the device, $\tilde{C}_\mathrm{u}$ the uniform feed concentration, and $\tilde{k}_\mathrm{on}$ the association rate, assuming that receptors in each reacting zone bind at the same rate. We scale the ligand concentration so that $\hat{C}(x, y, z, t)$ represents the dimensionless ligand depletion from the uniform ligand concentration.

## 2.1 Governing Equations

For biosensor devices, the channel height $\tilde{H}$ is much smaller than the device length $\tilde{L}$ and width $\tilde{W}$. With the Reynolds number $Re \ll 1$ for biosensor device parameters displayed in Table 1, we obtain a parabolic velocity profile for steady unidirectional Poiseuille flow between stationary plates with characteristic velocity $\tilde{V}$ (Zumbrum, submitted). Though the geometry is two-dimensional, it can be shown through conformal mapping arguments (Zumbrum and Edwards, submitted) that the flow is nearly unidirectional in the region containing reacting zones. Moreover, since $\tilde{H} \ll \tilde{W}$, the boundary layer along the sealed walls (see Fig. 1) is too thin to overlap the reacting zones. Hence to leading order, velocity variations in $z$ can be ignored.

**Table 1** Obtained and calculated parameter values for optical biosensor experiments

| Parameter | Value | Reference |
|---|---|---|
| $\tilde{C}_u$ (mol/cm$^3$) | $2.96 \times 10^{-12} - 2 \times 10^{-10}$ | Rich et al. (2008) |
| $\tilde{D}$ (cm$^2$/s) | $6.94 \times 10^{-6}$ | Rich et al. (2008) |
| Da | $1.11 \times 10^{-6} - 5.76$ | |
| $\tilde{H}$ (cm) | 0.018 | GE Healthcare (2006) |
| $K$ | $5 \times 10^{-5} - 3.38 \times 10^{4}$ | |
| $\tilde{k}_{off}$ (1/s) | $10^{-5} - 10^{-2}$ | GE Healthcare (2006) |
| $\tilde{k}_{on}$ (cm$^3$/mol s) | $10^{5} - 10^{9}$ | GE Healthcare (2006) |
| $\tilde{L}$ (cm) | 2.7 | Rich et al. (2008) |
| $\tilde{L}_r$ (cm) | $1.50 \times 10^{-2} - 3.50 \times 10^{-2}$ | GE Healthcare (2006) |
| Pe | $4.94 \times 10^{2} - 1.73 \times 10^{4}$ | |
| $\tilde{R}$ (mol/cm$^2$) | $1.11 \times 10^{-13} - 2.33 \times 10^{-11}$ | Rich et al. (2008) |
| $Re$ | $\leq 0.067$ | |
| $\tilde{V}$ (cm/s) | $3.70 \times 10^{-1} - 5.56$ | |
| $\tilde{W}$ (cm) | 1.5 | Rich et al. (2008) |

The large value of the Peclét number $\mathrm{Pe} = \tilde{V}\tilde{H}^2/\tilde{D}\tilde{L}_r$ in Table 1 indicates that the concentration only in a thin "unstirred" layer near the reacting surface contributes to the reaction. In this boundary layer, the velocity is linear, and the leading-order convection–diffusion equation is given by

$$\frac{\partial^2 \hat{C}}{\partial \eta^2} = \eta \frac{\partial \hat{C}}{\partial x}, \tag{2}$$

where the choice of scaling $y = \mathrm{Pe}^{-1/3}\eta$ removes the coefficient on the right-hand side of (2). Note also that due to the small aspect ratio $\tilde{H}/\tilde{W}$, diffusion in the $z$-direction may be neglected. Therefore, each streamline may be considered separately, causing $z$ to appear only as a parameter. (2) must be solved subject to the boundary condition for no depletion at the inlet

$$\hat{C}(0, \eta, t; z) = 0 \tag{3}$$

and the far-field condition for no depletion as $\eta \to \infty$

$$\hat{C}(x, \infty, t; z) = 0. \tag{4}$$

The rate of change of bound ligand depends simply on binding and unbinding of ligand and receptors, given by the dimensionless kinetics equation

$$\frac{\partial B}{\partial t} = (1 - B)[1 - \hat{C}(x, 0, t; z)] - KB, \quad (x, z) \in \mathcal{R}_r, \tag{5}$$

where $\mathcal{R}_r$ denotes the reacting surface. (Note that since $B$ is defined only on this reacting surface, we suppress its arguments here and in similar equations below.) Here we have scaled $\tilde{B}$ by the uniform receptor concentration $\tilde{R}$, and $K = \tilde{k}_{off}/\tilde{C}_u\tilde{k}_{on}$ is a scaled affinity constant. For no initial bound receptors, we have the initial condition

$$B(x, 0; z) = 0. \tag{6}$$

With no vertical convection within the channel, ligand and receptors interact due to diffusion. Therefore, diffusive flux into the surface must equal the rate of change of bound ligand concentration given by

$$\frac{\partial \hat{C}}{\partial \eta}(x, 0, t; z) = -\mathrm{Da}\frac{\partial B}{\partial t} I, \tag{7}$$

where the indicator function $I$ is defined by

$$I(x, z) = \begin{cases} 1, & (x, z) \in \mathcal{R}_r \\ 0, & (x, z) \notin \mathcal{R}_r, \end{cases} \tag{8}$$

since we have flux only over a reacting zone. In (7), we include the Damköhler number

$$\mathrm{Da} = \frac{k_{on}\mathrm{Pe}^{1/3}}{D\mathrm{Pe}^{2/3}} = \tilde{k}_{on}\tilde{R}\left(\frac{\tilde{H}\tilde{L}_r}{\tilde{D}^2\tilde{V}}\right)^{1/3},$$

which is the ratio of the rate of reaction to the rate of diffusion. Da measures the significance of transport effects; hence experimentalists want to drive Da as small as possible to isolate the pure reaction kinetics (Edwards 2001). Motivated by the bulk of the range in Table 1, we focus on the reaction-limited problem where $\mathrm{Da} \ll 1$.

Considering the leading-order Eqs. (2)–(4), (7) with $\mathrm{Da} = 0$, there is no leading-order ligand depletion. To obtain the leading-order bound state, we use the perturbation expansion

$$B(x, t; z) = B_0(x, t; z) + \mathcal{O}(\mathrm{Da}) \tag{9}$$

in (5) with the initial condition (6) to obtain the spatially uniform solution

$$B_0(t) = \frac{1 - e^{-(1+K)t}}{1 + K}, \tag{10}$$

corresponding to the well-mixed, spatially independent case.

Motivated by the form of (7), we let $\hat{C} = \mathrm{Da}C$ in (2)–(4), (7) to obtain the following system:

$$\frac{\partial^2 C}{\partial \eta^2} = \eta \frac{\partial C}{\partial x}, \tag{11}$$

$$C(0, \eta, t; z) = 0,$$

$$C(x, \infty, t; z) = 0,$$

$$\frac{\partial C}{\partial \eta}(x, 0, t; z) = -\frac{\partial B}{\partial t} I. \tag{12}$$

Note that with Da small, this substitution implies that the amount of ligand used in reactions is small enough to be neglected at leading order. We use the Laplace transform to solve (11) with the inlet concentration condition and boundary layer matching condition, and obtain the $\mathcal{O}(\mathrm{Da})$ ligand depletion

$$C(x, 0, t; z) = \frac{1}{3^{1/3}\Gamma(2/3)} \int_0^x \frac{\partial B}{\partial t}(\nu; z) I(\nu, z)(x - \nu)^{-2/3} \, \mathrm{d}\nu. \tag{13}$$

For the $i$th reacting zone with upstream and downstream boundaries $x_i^-(z)$ and $x_i^+(z)$, respectively, we include $z$ dependence due to the two-dimensional reacting zone but suppress explicit dependence below. For $x$ in the $i$th reacting zone, we integrate over reacting zones in a particular column and write the $i$ integrals over individual zones separately. Using (9) and the fact that $B_0$ is spatially uniform, we see that to leading order we may factor the bound state derivative out of the integral to obtain

$$C(x, 0, t; z) = \frac{\mathrm{d}B_0}{\mathrm{d}t} h(x; z) + \mathcal{O}(\mathrm{Da}), \tag{14}$$

where

$$h(x; z) = \frac{3^{2/3}}{\Gamma(2/3)} \left( \sum_{n=1}^{i-1} h_{n,i}(x; z) + h_{i,i}(x; z) \right), \tag{15}$$

for $h_{n,i}(x; z) = (x - x_n^-)^{1/3} - (x - x_n^+)^{1/3}$ and $h_{i,i}(x; z) = (x - x_i^-)^{1/3}$. We define $h_{n,i}$ for the ligand depletion over a streamline for an upstream reacting zone, which does not change as $x$ changes within the $i$th reacting zone; we define $h_{i,i}$ separately to account for changing $x$ which corresponds to different points along the streamline in the $i$th reacting zone. For the first row $i = 1$ of reacting zones, $h(x; z) = 3^{2/3} h_{1,1}/\Gamma(2/3)$.

## 2.2 Sensogram

With the inclusion of the bound state expansion (9) and the ligand depletion expression (14), Eq. (5) is

$$\frac{\partial B}{\partial t} = 1 - (1+K)B - \mathrm{Da}(1-B_0)\frac{\mathrm{d}B_0}{\mathrm{d}t}h(x;z) + \mathcal{O}(\mathrm{Da}^2). \tag{16}$$

Optical biosensors produce output for the average bound ligand concentration over a reacting zone, and we average the bound ligand concentration $B$ for an individual reacting zone to obtain a time-dependent sensogram. Since each row has a distinct average ligand depletion and sensogram, we use the notation $S_i[B]$ to represent the sensogram for a reacting zone $\mathcal{R}_i$ in the $i$th row so that

$$S_i[B] = \frac{1}{A}\iint_{\mathcal{R}_i} B\,\mathrm{d}A. \tag{17}$$

We average (16) to obtain

$$\frac{\mathrm{d}S_i[B]}{\mathrm{d}t} = 1 - (1+K)S_i[B] - \mathrm{Da}S_i[h](1-S_i[B_0])\frac{\mathrm{d}S_i[B_0]}{\mathrm{d}t} + \mathcal{O}(\mathrm{Da}^2),$$

where the average of the product $hB_0(\mathrm{d}B_0/\mathrm{d}t)$ is the product of the averages since $B_0$ is spatially uniform. We use manipulations similar to those in Zumbrum (submitted) with an $\mathcal{O}(\mathrm{Da}^2)$ error to relate the sensogram of the leading-order bound state and its derivative to the sensogram, and obtain the effective rate constant (ERC) equation

$$\frac{\mathrm{d}S_i[B]}{\mathrm{d}t} = (1-(1+K)S_i[B])\,(1-\mathrm{Da}_i(1-S_i[B])) + \mathcal{O}(\mathrm{Da}^2) \tag{18}$$

with initial condition $S_i[B](0) = 0$. The effective Damköhler number $\mathrm{Da}_i = \mathrm{Da}S_i[h]$ incorporates both zone placement and geometry for ligand depletion. It can be shown that $S_i[h] > S_{i-1}[h]$, so $\mathrm{Da}_i$ increases as one moves downstream: $\mathrm{Da}_i > \mathrm{Da}_{i-1}$.

Using the initial condition, we have from (18) that to leading order,

$$\frac{\mathrm{d}S_i[B]}{\mathrm{d}t}(0) = 1 - \mathrm{Da}_i;$$

hence to maintain a nonnegative bound ligand concentration $S_i[B]$ we must have that $\mathrm{Da}_i < 1$, or

$$\mathrm{Da} < 1/S_i[h]. \tag{19}$$

Given the ordering of the $S_i$, we see that (19) guarantees that $S_n[B] > 0$ for all $n \le i$. Note that (19) results from the way we averaged (16), and not from the model itself. However, recall that we are continually working in the limit that $\mathrm{Da} \ll 1$; hence (19) is really just a quantification on how small that is. There are other ways to average (discussed further in §4.3), but these have drawbacks as well.

We solve (18) using partial fractions to obtain

$$S_i[B] = \frac{1 - e^{-(1+(1-\mathrm{Da}_i)K)t}}{1 + K + \frac{\mathrm{Da}_i}{1-\mathrm{Da}_i}e^{-(1+(1-\mathrm{Da}_i)K)t}} + \mathcal{O}(\mathrm{Da}^2). \tag{20}$$

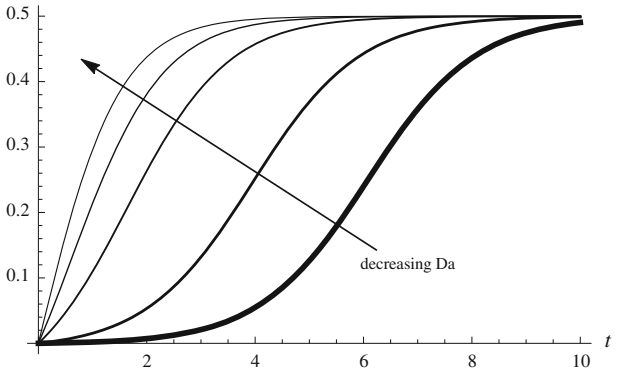


**Fig. 4** Sensograms $S_1[B]$ for Da $= 0.867, 0.86, 0.8, 0.7, 0.57$ (decreasing thickness) and $K = 1$. We see that a bound on the Damköhler number is necessary to produce a sensogram with the correct concavity

Note that the steady-state solution $1/(1+K)$ is stable, and while we make an $\mathcal{O}(\mathrm{Da}^2)$ error using a perturbation expansion for the bound state in (20), we expect this error to be small for $\mathrm{Da} \ll 1$. We expect (20) to exhibit properties reflective of the actual kinetics; namely that the bound ligand concentration increases until reaching equilibrium and that the rate of change of bound ligand decreases as receptors bind, so that $S_i[B]$ is increasing and $\mathrm{d}S_i[B]/\mathrm{d}t$ is decreasing. The former is guaranteed by (19); it can be shown in a similar manner that requiring $\mathrm{Da} < (1+K)/((2+K)S_i[h])$ is sufficient to obtain the correct downward concavity for the graph of the sensogram. This bound is more restrictive than the bound from the first derivative, but not concerning for the reaction-limited case under consideration.

As an example of the necessity of this bound, Fig. 4 contains sensograms for various Damköhler numbers over a single unit rectangular zone. (For this zone type $S_1[h] = 1.15209$; details for this calculation will be discussed in §3.) For plotting purposes, we may choose a value of $K$ based on the feed concentration $\tilde{C}_\mathrm{u}$ and take $K = 1$ for simplicity, yielding the bound $\mathrm{Da} < 2/(3(1.15209)) = 0.579$. We see that the sensogram concavity is only correct for the appropriate Da.

## 3 Reacting Zone Geometry and the Effective Damköhler Number

While we have an explicit sensogram expression for individual reacting zones within an array column, we now discuss the calculation and importance of the effective Damköhler number $\mathrm{Da}_i$. Though we are particularly interested in the case of an array of circular reacting zones in the Flexchip displayed in Fig. 3, we consider a more general case. In particular, we define the boundary of the reacting zone in the $i$th row and $j$th column generally as

$$\left(x - \left(\frac{1}{2} + 2(i-1)\right)\right)^{2m} + \left(z - \left(\frac{1}{2} + 2(j-1)\right)\right)^{2m} = \left(\frac{1}{2}\right)^{2m}, \; m = 1, 2, \ldots.$$

Hence, the case of circular reacting zones corresponds to $m = 1$ and the case of square zones corresponds to $m \to \infty$. Note that we define a column of reacting zones to be parallel to the flow and a row of reacting zones to be normal to the flow. As a function of $z$, the boundary of the reacting zone in the $i$th row and $j$th column is

$$x_i^{\pm}(z; j) = \frac{1}{2} + 2(i-1) \pm r(z; j), \tag{21}$$

where

$$r(z; j) = \sqrt[2m]{\frac{1}{2^{2m}} - \left(z - \left(\frac{1}{2} + 2(j-1)\right)\right)^{2m}}.$$

This zone boundary definition is especially useful for the case of circular reacting zones and square reacting zones but could be redefined for more general reacting zone geometries.

### 3.1 Expressions for the Effective Damköhler Number

With a definition for reacting zone boundaries, we compute the effective Damköhler number for individual reacting zones for general $m$, obtaining separate expressions for $\mathrm{Da}_1$ and $\mathrm{Da}_i$, $i > 1$.

#### *3.1.1 $Da_1$*

For the first row of reacting zones corresponding to $i = 1$, we have

$$\mathrm{Da}_1 = \mathrm{Da} S_1[h] = \frac{\mathrm{Da}}{A} \int_{z_j^-}^{z_j^+} \int_{x_1^-}^{x_1^+} h_{1,1}(x; z)\, \mathrm{d}x\, \mathrm{d}z.$$

Using the expressions for $x_1^-$ and $x_1^+$, we obtain a result in terms of gamma functions

$$\mathrm{Da}_1 = \frac{\mathrm{Da}\overline{h}}{A} \frac{2\Gamma(2/3m)\Gamma(1/2m)}{7m\Gamma(7/6m)}.$$

Note that $\overline{h} = 3^{5/3}/4\Gamma(2/3)$ corresponds to $S_1[h]$ for a single unit square reacting zone. For the reacting zone area $A$, we use a similar procedure to obtain

$$A = \int_{z_j^-}^{z_j^+} \int_{x_i^-}^{x_i^+} \mathrm{d}x\, \mathrm{d}z = \frac{\Gamma(1/2m)\Gamma(1/2m)}{4m\Gamma(1/m)}, \tag{22}$$

so that the effective Damköhler number for the first row of reacting zones as a function of the reacting zone boundary parameter $m$ is

$$\mathrm{Da}_1 = \mathrm{Da}\bar{h}\frac{8\Gamma(1/m)\Gamma(2/3m)}{7\Gamma(1/2m)\Gamma(7/6m)}. \tag{23}$$

*3.1.2 $Da_i$, $i > 1$*

In similar fashion, we compute the effective Damköhler number for downstream zones beyond the first row. For a reacting zone in row $i > 1$, we have

$$\mathrm{Da}_i = \mathrm{Da}S_i[h] = \frac{\mathrm{Da}}{A}\int_{z_j^-}^{z_j^+}\int_{x_i^-}^{x_i^+}\left(\sum_{n=1}^{i-1} h_{n,i}(x;z) + h_{i,i}(x;z)\right)\mathrm{d}x\,\mathrm{d}z.$$

We cannot write a simple expression for $\mathrm{Da}_i$ in terms of gamma functions as we did for $\mathrm{Da}_1$, but by changing variables and simplifying the sums, we can write the effective Damköhler number for downstream zones in the $i$th row as

$$\begin{aligned}\mathrm{Da}_i = \mathrm{Da}_1 + \frac{\mathrm{Da}\bar{h}}{A}\Bigg[&\sum_{n=1}^{i-1}\int_0^1\left(2n + \sqrt[2m]{1-x^{2m}}\right)^{4/3}\mathrm{d}x - \sum_{n=1}^{i-1}2(2n)^{4/3}\\ &+\sum_{n=1}^{i-1}\int_0^1\left(2n - \sqrt[2m]{1-x^{2m}}\right)^{4/3}\mathrm{d}x\Bigg].\end{aligned} \tag{24}$$

The effective Damköhler number increases with $i$, which corresponds to additional reacting zones in a column, leading to greater depletion accounted for in $\mathrm{Da}_i$. As a consequence of increased depletion and $\mathrm{Da}_i$, $\mathrm{d}S_i[B]/\mathrm{d}t$ in (18) decreases, slowing the rate of binding for the $i$th reacting zone.

*3.1.3 Effective Damköhler Number Comparison*

We calculate the ratio of $\mathrm{Da}_i$, $i > 1$, to $\mathrm{Da}_1$ to examine the change in the effective Damköhler number as $m$ increases and display the results in Fig. 5 for $i = 2, 3, 4, 5$. As $i$ increases for additional upstream zones, the ratio increases at a decreasing rate due to additional ligand depletion accounting for a smaller fraction of total ligand depletion. For fixed $i$, the ratio quickly asymptotes to the value of the ratio as $m \to \infty$ due to the reacting zone boundary definition, which suggests asymptotic expansions of the effective Damköhler number for large $m$ may be reasonable for $m \geq 1$.

This behavior for fixed $i$ and varying $m$ occurs due to the shape of the reacting zone. To illustrate this point, we simplify our discussion to a circular reacting zone ($m = 1$) and a square reacting zone ($m \to \infty$), displayed in Fig. 6. Depletion occurs along horizontal streamlines from the left boundary to the right boundary of each zone, and streamlines are longer in the square zone than the circular zone. Hence, reactions that

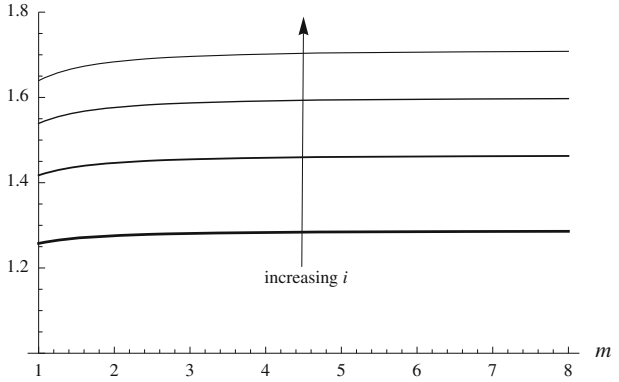


**Fig. 5** Ratio of $\mathrm{Da}_i$ to $\mathrm{Da}_1$ for $i = 2, 3, 4, 5$. Note that zones further down the channel have a larger effective Damköhler number, corresponding to increased depletion

occur in the shaded regions for only the square zone exacerbate the depletion effect. For any two reacting zones corresponding to different $m$ values, a similar argument holds so that depletion is greater for the zone corresponding to the larger $m$ value.

This shape effect is more pronounced for small $m$, since the reacting zone boundary changes most significantly for small $m$. This is evident in the derivative of the ratio, which increases with $i$ due to the cumulative depletion effect for multiple reacting zones in a row. An increased $m$ yields additional depletion not only for the zone of interest but also for all upstream zones, so the ratio changes quickly for small $m$ as $i$ increases. As $m$ increases through moderate values, the shape of the reacting zone quickly resembles the square zone; hence, additional ligand depletion from this shape effect is minimal for moderate values of $m$.

## 3.2 Square Reacting Zones

To verify our results, we may take the limit as $m \to \infty$ (square zones) and show that the resulting leading-order expressions match results from the one-dimensional model by Edwards (2011).

### *3.2.1 $Da_1$*

To examine the behavior of $\mathrm{Da}_1$ as $m \to \infty$, we use the Laurent expansion for the gamma function so that

$$\mathrm{Da}_1 = \mathrm{Da}\overline{h}\left(1 - \frac{\pi^2}{72m^2}\right) + \mathcal{O}\left(\frac{1}{m^3}\right), \tag{25}$$

which is valid for $m > 1$. For large $m$, $\mathrm{Da}_1$ approaches $\mathrm{Da}\overline{h}$ for a single zone as we expect. Figure 7 contains a plot of the ratio of the asymptotic value of $\mathrm{Da}_1$ in (25) to the exact value of $\mathrm{Da}_1$ in (23) for $m \geq 1$. We see that the difference between the asymptotic

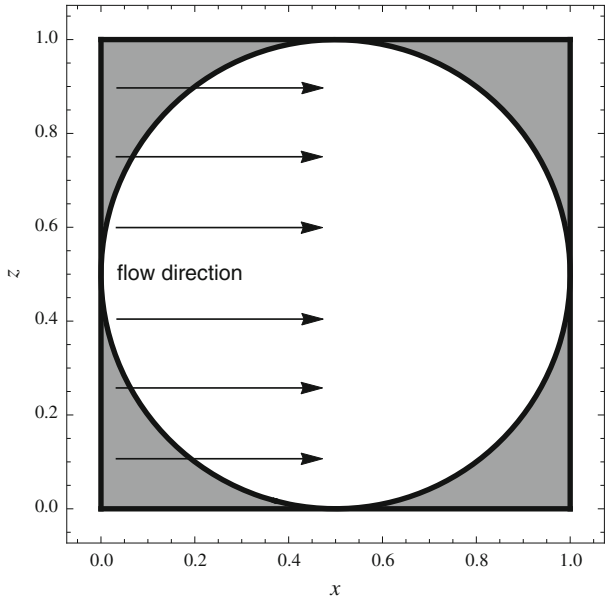


**Fig. 6** Representation of a circular and square reacting zone with non-overlapping regions shaded

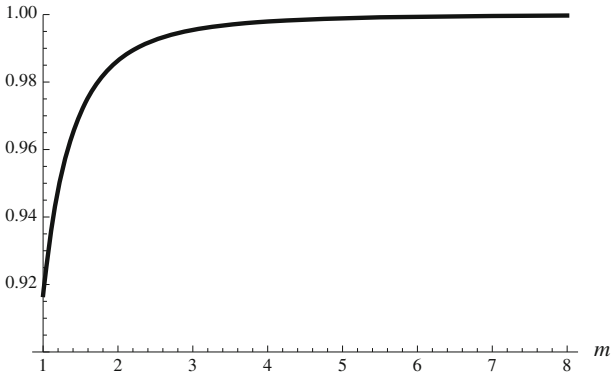


**Fig. 7** Ratio of the asymptotic value of $\mathrm{Da}_1$ to the exact value of $\mathrm{Da}_1$ for various $m$

and exact value is less than 9% regardless of the Damköhler number and parameter $m$; since this difference is minimal and biosensor results contain experimental noise, this asymptotic expression could serve as a reasonable approximation for any reacting zone geometry with $m \geq 1$.

### *3.2.2 $Da_i, i > 1$*

Computing the effective Damköhler number for additional rows, we consider the first term in (24) to show behavior for large $m$. Using the Maclaurin series for the radical function and integrating term-by-term, we obtain

$$\int_0^1 \left(2n + \sqrt[2m]{1-x^{2m}}\right)^{4/3} \mathrm{d}x = (2n+1)^{4/3} - \frac{2(2n+1)^{1/3}}{3m} H_{1/2m} + \mathcal{O}\left(\frac{1}{m^3}\right),$$

where $H_{1/2m}$ is the harmonic number of argument $1/2m$. Similarly for the third term in (24), we have

$$\int_0^1 \left(2n - \sqrt[2m]{1-x^{2m}}\right)^{4/3} \mathrm{d}x = (2n-1)^{4/3} + \frac{2(2n-1)^{1/3}}{3m} H_{1/2m} + \mathcal{O}\left(\frac{1}{m^3}\right).$$

Using these expressions and simplifying the telescoping coefficients for the sum over $k$, we obtain the asymptotic expression

$$\mathrm{Da}_i \sim \mathrm{Da}_1 + \frac{\mathrm{Da}\bar{h}}{A}\left[\sum_{n=1}^{i-1}\left((2n+1)^{4/3} - 2(2n)^{4/3} + (2n-1)^{4/3}\right) + \frac{2\left(1-(2i-1)^{1/3}\right)}{3m} H_{1/2m}\right].$$

In Fig. 8, we display the ratio of the asymptotic value of $\mathrm{Da}_i$ to the exact value of $\mathrm{Da}_i$ and observe that the difference is minimal for reacting zones in rows $i = 2, 3, 4, 5$; for a reacting zone with $m \geq 1$ in the 20th row, this difference is less than 8%.

For large $m$, we neglect the $\mathcal{O}(1/m^2)$ correction for $\mathrm{Da}_i$ and use that $\mathrm{Da}_1$ is asymptotic to $\mathrm{Da}\bar{h}/A = \mathrm{Da}\bar{h}$ for square reacting zones with $A = 1$ to obtain the effective Damköher number given by

$$\begin{aligned}\mathrm{Da}_i &= \mathrm{Da}_1\left[1 + \sum_{n=1}^{i-1}\left((2n-1)^{4/3} - 2(2n)^{4/3} + (2n+1)^{4/3}\right)\right] \\ &= \mathrm{Da}_1\left[(2i-1)^{4/3} + 2\sum_{n=1}^{2i-2}(-1)^{n-1}n^{4/3}\right],\end{aligned}$$

which is the result for the one-dimensional case given by Edwards (2011) in Eq. (3.16a). To provide a sense of effective Damköhler number values, Table 2 displays $\mathrm{Da}_i$ for the first five rows of square reacting zones with $\mathrm{Da} = 0.1$. The effective Damköhler number increases with $i$ as additional upstream zones deplete ligand, but this is not concerning since the constant $\mathrm{Da}_i$ is included in the argument of exponentially decaying terms in the sensogram (20).

### *3.2.3 Sensograms*

Using the result for $\mathrm{Da}_i$ in the limit as $m \to \infty$ and $K = 1$, we plot the leading-order bound state and sensogram $S_5[B]$ for reacting zones in row $i = 5$ from (20) in the inset of Fig. 9. We observe the $\mathcal{O}(\mathrm{Da})$ effect included in the sensogram and note

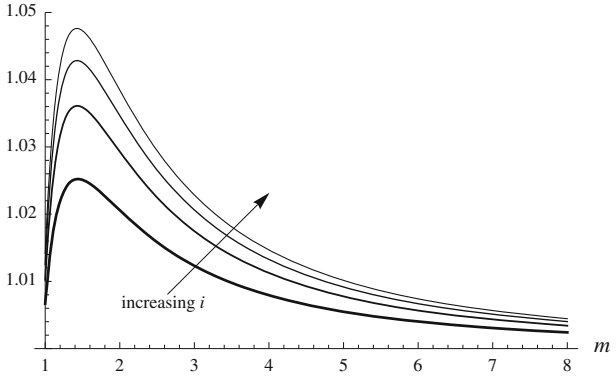


**Fig. 8** Ratio of the asymptotic value of $\mathrm{Da}_i$ to the exact value of $\mathrm{Da}_i$ for various $m$, $i = 2, 3, 4, 5$

**Table 2** Effective Damköhler number for the first five rows of square reacting zones with $\mathrm{Da} = 0.1$

| $i$ | 1 | 2 | 3 | 4 | 5 |
|---|---|---|---|---|---|
| $\mathrm{Da}_i$ | 0.115209 | 0.148281 | 0.168721 | 0.184269 | 0.197089 |

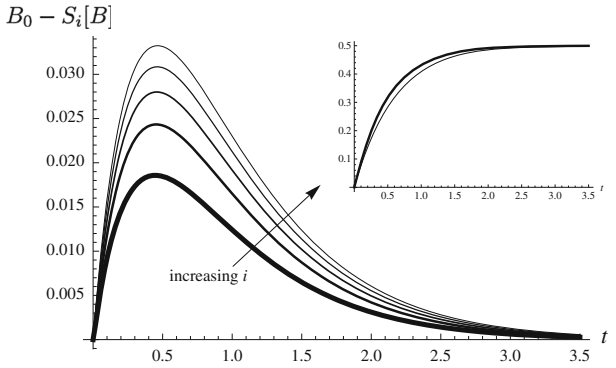


**Fig. 9** For $\mathrm{Da} = 0.1$ and $K = 1$, difference $B_0 - S_i[B]$ for $i = 1, 2, 3, 4, 5$ for square reacting zones. Inset: Leading-order bound state (*thick line*) and sensogram (20) for $i = 5$ (*thin line*). Note that as $i$ increases, binding slows, reflecting increased depletion further down the channel

that as the effective Damköhler number increases with additional ligand depletion, the sensogram derivative in Eq. (18) decreases. Therefore, the reaction slows and the bound state decreases.

To examine how the sensogram $S_i[B]$ changes as $i$ increases with additional upstream zones, we consider the difference $B_0 - S_i[B]$ between the leading-order bound state and sensogram in Fig. 9. For additional upstream zones, this difference increases due to additional ligand depletion, but at a decreasing rate since the additional depletion is a smaller fraction of total depletion for additional rows. This behavior is due to the corresponding behavior of the effective Damköhler number for increased $i$.

**Table 3** Effective Damköhler number for the first five rows of circular reacting zones with Da = 0.1

| $i$ | 1 | 2 | 3 | 4 | 5 |
|---|---|---|---|---|---|
| $\mathrm{Da}_i$ | 0.108428 | 0.136355 | 0.153685 | 0.166875 | 0.177754 |

### 3.3 Circular Reacting Zones

Rectangular reacting zones are convenient to analyze mathematically, as the governing equations simplify to a one-dimensional model. However, in this manuscript we wish to consider the more experimentally relevant case of circular zones, as seen in such devices as the Flexchip and dotLab. To understand the effect of circular reacting zones, we consider the case of $m = 1$ in the definition of the reacting zone boundaries. To generate sensograms for circular reacting zones, we include this zone geometry in the effective Damköhler number. While the asymptotic expressions derived in the limit of large $m$ were reasonable for $m \geq 1$, we compute the effective Damköhler numbers for the specific case $m = 1$.

#### *3.3.1 $Da_1$*

From (23), the effective Damköhler number for circular reacting zones in the first row $i = 1$ is $\mathrm{Da}_1 = 3^{2/3}\mathrm{Da}/\sqrt{\pi}\Gamma(13/6)$. Here the reacting zone area in (22) $A = \Gamma(1/2)\Gamma(1/2)/4\Gamma(1)$ of course reduces to $A = \pi/4$.

#### *3.3.2 $Da_i, i > 1$*

From (24), we numerically compute the effective Damköhler number for circular reacting zones in row $i > 1$. Table 3 displays effective Damköhler numbers for the first five rows of circular reacting zones with Da = 0.1, and we see a decrease in the effective Damköhler number from Table 2 for the corresponding square zones due to less ligand depletion as previously discussed.

#### *3.3.3 Sensograms and Comparison with Sensograms for Square Reacting Zones*

Plotting the sensogram (20) for circular reacting zones, we see similar behavior to square zones. Figure 10 displays the leading-order bound state and sensogram $S_5[B]$ in the inset, and the difference between the leading-order bound state and sensogram for the first five rows of reacting zones.

Comparing the sensograms $S_i[B]$ for circular and square reacting zones, we see that the difference $S_i[B]_{m=1} - S_i[B]_{m\to\infty}$ in Fig. 11 is nonnegative for all reacting zones, which can be directly attributed to the effective Damköhler number and reacting zone geometry. Circular zones have less ligand depletion, smaller effective Damköhler numbers, and consequently larger bound states than square zones. Note though that this difference is extremely small compared to the corresponding sensogram and difference from the leading-order bound state.

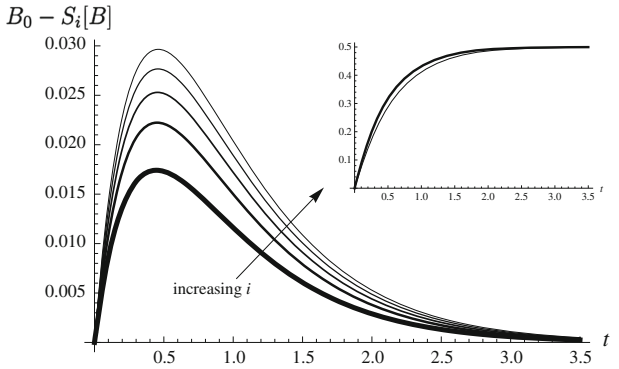


**Fig. 10** For Da $= 0.1$ and $K = 1$, difference $B_0 - S_i[B]$ for $i = 1, 2, 3, 4, 5$ for circular reacting zones. Inset: Leading-order bound state (*thick line*) and sensogram (20) for $i = 5$ (*thin line*). Again as $i$ increases, binding slows, reflecting increased depletion further down the channel

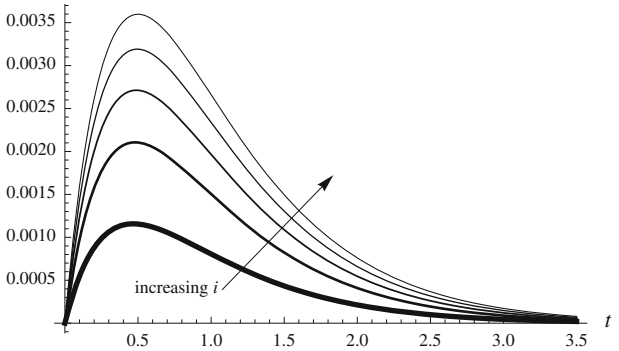


**Fig. 11** Sensogram difference $S_i[B]_{m=1} - S_i[B]_{m\to\infty}$ corresponding to circular and square reacting zones for $i = 1, 2, 3, 4, 5$. The difference is positive due to additional depletion along streamlines over square zones compared to circular zones (as discussed in §3.1.3) and is increased with $i$ as this additional depletion effect accumulates

## 3.4 Calculation of Rate Constants

In the previous section, we produced sensograms for circular reacting zones within an array column, highlighting the effect that row placement has on sensogram behavior due to ligand depletion. However, experimentalists are most interested in obtaining rate constants from sensogram data. To examine rate constant estimates and row placement effects, we include rate constants in the sensogram (20) using the dimensional time scale $\tilde{t}$ and the definition for $K$ to obtain the dimensional expression

$$S_i[B](\tilde{t}) = \frac{\tilde{C}_u\tilde{k}_{on}(1 - e^{-(\tilde{C}_u\tilde{k}_{on}+(1-\mathrm{Da}_i)\tilde{k}_{off})\tilde{t}})}{\tilde{C}_u\tilde{k}_{on} + \tilde{k}_{off} + \tilde{C}_u\tilde{k}_{on}\frac{\mathrm{Da}_i}{1-\mathrm{Da}_i}e^{-(\tilde{C}_u\tilde{k}_{on}+(1-\mathrm{Da}_i)\tilde{k}_{off})\tilde{t}}}. \tag{26}$$

**Table 4** Estimated rate constants for reacting zones in rows 1, 2, 3, 4, 5, and 20 using the naïve one-row approach; the exact value is 10 in each case. Due to depletion of the ligand, using the naïve one-row approach significantly understates the rate constants in downstream zones

| $i$ | 1 | 2 | 3 | 4 | 5 | 20 |
|---|---|---|---|---|---|---|
| $\tilde{k}_{\text{on}}$ ($10^6$ cm$^3$/mol s) | 9.99788 | 9.75023 | 9.59607 | 9.47846 | 9.38128 | 8.61153 |
| $\tilde{k}_{\text{off}}$ ($10^{-5}$ s$^{-1}$) | 9.99757 | 9.74042 | 9.57998 | 9.45738 | 9.35594 | 8.54739 |

We consider circular reacting zones with Da $= 0.1$ and $K = 1$ and assume values for the uniform feed concentration $\tilde{C}_{\text{u}} = 10^{-11}$ mol/cm$^3$ and rate constants

$$\tilde{k}_{\text{on}} = 10^7 \text{ cm}^3/\text{mol s} \text{ and } \tilde{k}_{\text{off}} = 10^{-4} \text{ s}^{-1}, \tag{27}$$

maintaining consistency with the choice of $K = 1$. With these parameter values, we calculate the sensograms $S_i[B](\tilde{t})$ from (26) for rows $i = 1, 2, \ldots, 20$ with $\tilde{t} \in [0, 35000]$ seconds and sample at integer times to obtain simulated sensogram data for twenty rows of reacting zones in the Flexchip. Note that the sensograms $S_i[B](\tilde{t})$ for $i = 1, 2, \ldots, 5$ correspond to those used to produce Fig. 10 on the reaction time scale $t \in [0, 3.5]$.

To determine how ignoring row placement distorts the measurement of rate constants, we fit (26) with $i = 1$ to the simulated sensogram data from row $i$ using the least-squares fitting command `FindFit` in Mathematica. In other words, we naïvely use the one-row model on each row, thereby neglecting the additional depletion for downstream rows. We compute the estimated rate constants displayed in Table 4, noting that the relative error for row 1 is less than 0.03%, which is due only to the parameter estimation.

For rows $i > 1$, the simulated data includes depletion effects along the channel from upstream zones, so we expect to obtain estimates for the rate constants that are smaller than those in (27). In Table 4, we include the estimated rate constants for zones in rows $i = 2, 3, 4, 5,$ and 20. We see that these values decrease with additional upstream zones, as expected due to our naïve model choice. In fact, the relative error for the 20th row is 15%, showing the importance of utilizing the multiple-row approach. Since $\mathcal{O}$(Da) transport effects are included in both the simulated data and the model to which the data is fitted, errors in the estimated rate constants in Table 4 are due only to depletion effects along the channel from upstream zones.

## 4 Array of Reacting Zones with Different Rate Constants

An advantage that the Flexchip offers is that an array of reacting zones allows for the testing of up to 400 different receptors in a single experiment (Rich et al. 2008). Each reacting zone contains a different receptor; hence in this situation, the rate constants in each zone will be different. Our model can handle this case easily. Still working in the case of unidirectional flow, we consider each column of reacting zones independently

and treat $z$ as a parameter. Therefore, the following work can be applied to any column of reacting zones.

### 4.1 Governing Equations

In this case, we must account for not only reacting zone geometry and row position within an array, but also differing rate constants $\tilde{k}_{\mathrm{on}_i}$, $\tilde{k}_{\mathrm{off}_i}$ for ligand-receptor interactions in the $i$th reacting zone. We use the dimensionless association rate $k_{\mathrm{on}_i} = \tilde{C}_{\mathrm{u}}\tilde{k}_{\mathrm{on}_i}\tilde{L}_{\mathrm{r}}/\tilde{V}$ in the Damköhler number ${}_i\mathrm{Da}$ for the $i$th reacting zone, with the leading subscript used to avoid confusion with the effective Damköhler number notation.

Equation (2) and conditions (3) and (4) for ligand depletion are the same, but since the reaction rate constants are different for each reacting zone, we have the following zone-specific dimensionless kinetics equation analogous to (5) for the $i$th reacting zone:

$$\frac{\partial B_i}{\partial t} = \kappa_{\mathrm{on}_i}\left[(1-B_i)(1-\hat{C}) - K_i B_i\right], \quad x \in \left[x_i^-(z), x_i^+(z)\right], \tag{28}$$

where $\kappa_{\mathrm{on}_i} = \tilde{k}_{\mathrm{on}_i}/\tilde{k}_{\mathrm{on}_1}$ and $K_i = \tilde{k}_{\mathrm{off}_i}/\tilde{C}_{\mathrm{u}}\tilde{k}_{\mathrm{on}_i}$. By definition, $\kappa_{\mathrm{on}_1} = 1$. We also have the dimensionless flux equation for the $i$th reacting zone

$$\frac{\partial \hat{C}}{\partial \eta}(x,0,t;z) = -{}_1\mathrm{Da}\frac{\partial B_i}{\partial t}, \tag{29}$$

analogous to (7).

Again, there is no leading-order ligand depletion, and with the perturbation expansion $B_i(x,t;z) = B_{i,0}(x,t;z) + \mathcal{O}({}_1\mathrm{Da}^2)$, we obtain the leading-order bound state

$$B_{i,0}(t) = \frac{1}{1+K_i}\left[1 - e^{-\kappa_{\mathrm{on}_i}(1+K_i)t}\right]. \tag{30}$$

Note that the steady-state solution for the leading-order bound state $1/(1+K_i)$ is not necessarily the same for different reacting zones.

In an analogous manner to that used in §2.1, we use the form of (29) to motivate the substitution $\hat{C} = {}_1\mathrm{Da}C$. We use the same variable $C$ as before to represent the depletion scaled by transport effects. The resulting expression for $C$ for unidirectional flow

$$C(x,0,t;z) = \begin{cases} \dfrac{3^{2/3}}{\Gamma(2/3)}\dfrac{\mathrm{d}B_{1,0}}{\mathrm{d}t}h_{1,1}, & x \in [x_1^-, x_1^+] \\ \dfrac{3^{2/3}}{\Gamma(2/3)}\left(\displaystyle\sum_{n=1}^{i-1}\frac{\mathrm{d}B_{n,0}}{\mathrm{d}t}h_{n,i} + \frac{\mathrm{d}B_{i,0}}{\mathrm{d}t}h_{i,i}\right), & x \in [x_i^-, x_i^+], \quad i > 1, \end{cases}$$

is similar to (14) with the exception that bound-state derivatives are zone-dependent and cannot be factored from the sum. Using the notation $g = 3^{2/3}/A\Gamma(2/3)$ and

$S[\cdot]$ without subscript since bound states are row-dependent, we obtain the averaged expression

$$S[C](t) = \begin{cases} g\dfrac{\mathrm{d}S[B_{1,0}]}{\mathrm{d}t}S[h_{1,1}], & x \in [x_1^-, x_1^+] \\ g\left(\displaystyle\sum_{n=1}^{i-1}\frac{\mathrm{d}S[B_{n,0}]}{\mathrm{d}t}S[h_{n,i}] + \frac{\mathrm{d}S[B_{i,0}]}{\mathrm{d}t}S[h_{i,i}]\right), & x \in [x_i^-, x_i^+], \quad i > 1, \end{cases} \tag{31}$$

which we use in the averaged kinetics equation

$$\frac{\mathrm{d}S[B_i]}{\mathrm{d}t} = \kappa_{\mathrm{on}_i}\left[1 - (1+K_i)S[B_i]\right] - \kappa_{\mathrm{on}_i}(1 - S[B_i])_1\mathrm{Da}S[C](t) + \mathcal{O}(_1\mathrm{Da}^2). \tag{32}$$

## 4.2 ERC Equation Analogous to (18)

In the term $_1\mathrm{Da}S[C](t)$, the bound-state derivative is zone-dependent, cannot be factored from the sum, and includes explicit time dependence so that (32) is not separable. To obtain an ODE of similar form as that for arrays of reacting zones with the same receptors, we isolate the upstream ligand depletion terms to obtain the ERC equation

$$\begin{aligned} \frac{dS[B_i]}{dt} = {} & \kappa_{\mathrm{on}_i}\left[1 - (1+K_i)\,S[B_i]\right]\left[1 - \kappa_{\mathrm{on}_i}{}_1\mathrm{Da}g S[h_{i,i}](1 - S[B_i])\right] \\ & -\kappa_{\mathrm{on}_i}{}_1\mathrm{Da}g(1 - S[B_i])\sum_{n=1}^{i-1}\kappa_{\mathrm{on}_n}e^{-\kappa_{\mathrm{on}_n}(1+K_i)t}S[h_{n,i}] + \mathcal{O}(_1\mathrm{Da}^2). \end{aligned} \tag{33}$$

We see that the term on the second line of (33) incorporates the upstream depletion, which slows the reaction, remains bounded, and approaches zero as $t \to \infty$. In the case of only one reacting zone, this term is not included and (33) simplifies to the ERC equation in Zumbrum (submitted).

As in the previous case, we must bound the Damköhler number to maintain the correct physical properties for a sensogram, namely that it remains nonnegative and concave down. For the sensogram to be nonnegative, $\mathrm{d}S[B_i]/\mathrm{d}t$ must be positive when $S[B_i] = 0$; for the sensogram to be concave down, $\mathrm{d}^2S[B_i]/\mathrm{d}t^2$ must be negative when $t = 0$. These requirements yield the respective bounds

$$_1\mathrm{Da} < \frac{1}{b}. \tag{34}$$

and

$$_1\mathrm{Da}^2 - \frac{a + bc + d}{bd}{}_1\mathrm{Da} + \frac{c}{bd} > 0,$$

for

$$a = \kappa_{\mathrm{on}_i} g \sum_{n=1}^{i-1} \kappa_{\mathrm{on}_n}^2 (1 + K_n) S[h_{n,i}], \quad b = g \sum_{n=1}^{i} \kappa_{\mathrm{on}_n} S[h_{n,i}], \quad c = \kappa_{\mathrm{on}_i}^2 (1 + K_i),$$

$$d = \kappa_{\mathrm{on}_i}^2 g \left( \kappa_{\mathrm{on}_i} (1 + K_i) S[h_{i,i}] + \sum_{n=1}^{i} \kappa_{\mathrm{on}_n} S[h_{n,i}] \right).$$

With roots ${}_1\mathrm{Da}_\pm = \left(a + bc + d \pm \sqrt{(a + bc + d)^2 - 4bcd}\right)/2bd$, the product $({}_1\mathrm{Da} - {}_1\mathrm{Da}_+)({}_1\mathrm{Da} - {}_1\mathrm{Da}_-)$ is positive when ${}_1\mathrm{Da} > {}_1\mathrm{Da}_+$ or ${}_1\mathrm{Da} < {}_1\mathrm{Da}_-$. It can be shown that the former bound allows nonphysical negative bound states and the latter is more restrictive than (34); hence, we require that

$${}_1\mathrm{Da} < {}_1\mathrm{Da}_- = \frac{a + bc + d}{2bd} \left[ 1 - \sqrt{1 - \frac{4bcd}{(a + bc + d)^2}} \right].$$

For large $\kappa_{\mathrm{on}_i}$, ${}_1\mathrm{Da}_-$ is asymptotic to $\kappa_{\mathrm{on}_i}^{-1}$. Since association rates for different reacting zones can differ by several orders of magnitude, the Da range for which (33) is applicable may be severely limited; hence experimentalists that wish to use this model would be forced to design analyses within this limited Da range. If instead the reacting zones have association rates that are closer in order of magnitude, the Da bound would be much less restrictive and would not require experimentalists to drive Da down as dramatically to use this model.

As an aside, we note that the manipulations that led to (33) all implicitly assumed that the rate constants are different in each zone. Hence (33) does not straightforwardly reduce to (18) in the case where all the reacting zones do have the same rate constants. However, since this case corresponds to zones with the same receptor, experimentalists would know *a priori* that this is the case. With regards to experimental design, if multiple reacting zones of the same receptor are to be studied, it is preferable to place the reacting zones with this receptor in the same column so that we may use (20) to model sensograms.

### 4.3 ERC Equation with Time-Dependent Effective Damköhler Number

We may also produce an ERC equation (similar to Edwards (2011)) with a time-dependent effective Damköhler number by scaling each term in the ligand depletion expression with respect to the leading-order bound state for the $i$th reacting zone. To do this, we factor $\mathrm{d}S[B_{i,0}]/\mathrm{d}t$ from each term of the summation in (31) and leave the corresponding exponential term from this factoring in the summand to obtain

$$\sum_{n=1}^{i-1} \frac{\mathrm{d}S[B_{n,0}]}{\mathrm{d}t} S[h_{n,i}] = \frac{1}{\kappa_{\mathrm{on}_i}} \frac{\mathrm{d}S[B_{i,0}]}{\mathrm{d}t} \sum_{n=1}^{i-1} e^{\kappa_{\mathrm{on}_i}(1+K_i)t} \frac{\mathrm{d}S[B_{n,0}]}{\mathrm{d}t} S[h_{n,i}].$$

We can write the averaged ligand depletion as

$$ {}_1\mathrm{Da}S[C](t) = \frac{1}{\kappa_{\mathrm{on}_i}} \frac{\mathrm{d}S[B_{i,0}]}{\mathrm{d}t} \mathrm{Da}_i(t), \tag{35} $$

where

$$ \mathrm{Da}_i(t) = {}_1\mathrm{Da}g \sum_{n=1}^{i} \kappa_{\mathrm{on}_n} e^{\kappa_{\mathrm{on}_i}(1+K_i)t - \kappa_{\mathrm{on}_n}(1+K_n)t} S[h_{n,i}] $$

and the constant $i$th summand is included since for $n = i$

$$ e^{\kappa_{\mathrm{on}_i}(1+K_i)t - \kappa_{\mathrm{on}_n}(1+K_n)t} = 1. \tag{36} $$

Using (35) and the fact that $S[B_i] = S[B_{i,0}] + \mathcal{O}({}_1\mathrm{Da})$ and $\mathrm{d}S[B_i]/\mathrm{d}t = \mathrm{d}S[B_{i,0}]/\mathrm{d}t + \mathcal{O}({}_1\mathrm{Da})$ in (32), we obtain

$$ \frac{\mathrm{d}S[B_i]}{\mathrm{d}t} = \kappa_{\mathrm{on}_i}\left[1 - (1+K_i)S[B_i]\right] - (1 - S[B_i]) \frac{\mathrm{d}S[B_i]}{\mathrm{d}t} \mathrm{Da}_i(t) + \mathcal{O}({}_1\mathrm{Da}^2), $$

with the sensogram computed numerically from

$$ \frac{\mathrm{d}S[B_i]}{\mathrm{d}t} = \frac{\kappa_{\mathrm{on}_i}\left[1 - (1+K_i)S[B_i]\right]}{1 + \mathrm{Da}_i(t)(1 - S[B_i])} + \mathcal{O}({}_1\mathrm{Da}^2). \tag{37} $$

The time-dependent effective Damköhler number $\mathrm{Da}_i(t)$ accounts for upstream zone position and geometry, as well as different rate constants. Working row by row, $\mathrm{Da}_i(t)$ is a known function, depending only on the leading-order bound state of the preceding $i - 1$ reacting zones.

In the case of only one reacting zone, $\mathrm{Da}_i(t) = \mathrm{Da}S[h]$, and (37) simplifies to (3.14) in Edwards (2011). In the case where the rate constants are the same for all reacting zones in a column, (36) holds for all $n$ so that $\mathrm{Da}_i(t)$ simplifies to $\mathrm{Da}_i$ for multiple zones with the same rate constants. With regards to experimental design, if multiple reacting zones of the same receptor are to be studied, it is preferable to place reacting zones with this receptor in the same column so that we may use results in §3.

Unfortunately, (37) also has a limitation with regards to its application. Physically, ${}_1\mathrm{Da}S[C](t)$ in (35) must be bounded between 0 and 1. Writing this term as the product of $\mathrm{d}S[B_{i,0}]/\mathrm{d}t$ and $\mathrm{Da}_i(t)$, we recognize that $\mathrm{d}S[B_{i,0}]/\mathrm{d}t$ is bounded and tends to 0 as $t \to \infty$, but $\mathrm{Da}_i(t)$ may be unbounded as $t \to \infty$ without certain conditions on the rate constants for reacting zones in different rows. Note that this is different from the case for an array of reacting zones with the same receptor where $\mathrm{Da}_i \to \infty$ for increasing $i$. For that case, $\mathrm{Da}_i$ is constant in time for a specific zone and increases only as we move between zones.

To guarantee the boundedness of $\mathrm{Da}_i(t)$, each exponential term must be bounded with

$$\kappa_{\mathrm{on}_i}(1+K_i) \leq \kappa_{\mathrm{on}_n}(1+K_n) \text{ for all } n < i. \tag{38}$$

In terms of the rate constants, we must order the reacting zones with $\tilde{C}_\mathrm{u}\tilde{k}_{\mathrm{on}_i} + \tilde{k}_{\mathrm{off}_i} \leq \tilde{C}_\mathrm{u}\tilde{k}_{\mathrm{on}_n} + \tilde{k}_{\mathrm{off}_n}$ for $n < i$. $\tilde{C}_\mathrm{u}\tilde{k}_{\mathrm{on}_i}$ and $\tilde{k}_{\mathrm{off}_i}$ may assume values on the ranges $\mathcal{O}(10^{-7})$ – $\mathcal{O}(10^{-1})$ and $\mathcal{O}(10^{-5})$ – $\mathcal{O}(10^{-2})$ respectively, meaning these terms may be the same order, as when we use $K = 1$ and $K_1 = 1$ for plotting, or one term may dominate if it is much larger than the other. For example, if $\tilde{C}_\mathrm{u}\tilde{k}_{\mathrm{on}_i} \gg \tilde{k}_{\mathrm{off}_i}$, reacting zones must be ordered by decreasing association rate to have $\mathrm{Da}_i(t)$ bounded. For the experimental setup of a column that satisfies this requirement, the zone closest to the inlet must contain the receptor with the largest association rate. Any additional zone placed downstream must have a smaller association rate than all preceding zones in the column. Ordering reacting zones within a column in this manner is difficult experimentally since the rate constants are the values to be found, and even with some *a priori* information about the rate constants, it would be challenging to satisfy this requirement.

The boundedness of $\mathrm{Da}_i(t)$ is important for using (37) to compute sensograms; if we do not satisfy (38) yet scale the ligand depletion with respect to the derivative of the bound state for the $i$th zone in (35), an unbounded term results in the denominator of (37). This term drives the derivative $\mathrm{d}S[B_i]/\mathrm{d}t$ to zero, resulting in an underestimate of the sensogram steady-state solution. In this case $\mathrm{d}S[B]/\mathrm{d}t = f_1(S[B], t)\, f_2(S[B])$ with $f_1(\cdot, t) \to 0$ as $t \to \infty$; hence the steady state is not necessarily given by $f_2(S[B]) = 0$.

For a simple two-zone example, consider circular reacting zones and a reacting zone in the second row with $\kappa_{\mathrm{on}_2} = 50$ and $K_2 = 1/50$, where the use of (37) is not appropriate since $\kappa_{\mathrm{on}_2}(1+K_2) = 51 > 2 = \kappa_{\mathrm{on}_1}(1+K_1)$. In Fig. 12, we display the leading-order bound state of the second reacting zone from (30) and the

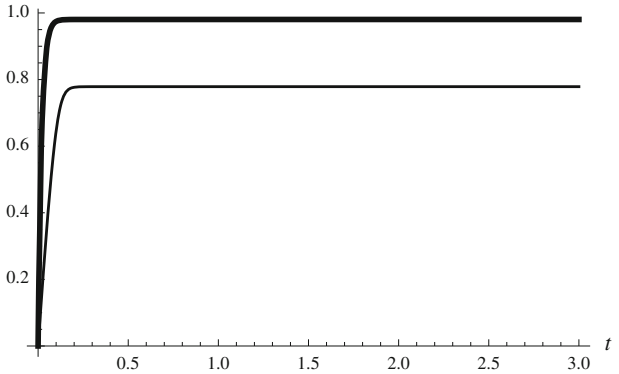


**Fig. 12** For ${}_1\mathrm{Da} = 0.1$, $K_1 = 1$, $\kappa_{\mathrm{on}_2} = 50$ and $K_2 = 1/50$, leading-order bound state for the second reacting zone from (30) (*thick line*) and sensogram from (37) for $i = 2$ (*thin line*). This example illustrates that if the bound in (38) is not satisfied, the model (37) does not produce the expected steady state

sensogram $S[B_2]$ from (37). The underestimation of the bound state occurs whenever the boundedness condition for $\mathrm{Da}_i(t)$ is not met, and we choose $\kappa_{\mathrm{on}_2} = 50$ for Fig. 12 to make this effect pronounced.

## 5 Conclusions

In order to accurately estimate rate constants from optical biosensors, one needs a reliable mathematical model for the underlying sensogram data. Most current analytical models of the Biacore have treated the device as one-dimensional (Edwards 1999, 2001, 2011; Hansen et al. 2012; Mason et al. 1999; Zumbrum, submitted). In the case of the Flexchip, a two-dimensional approach is required if one considers the true case of circular reacting zones.

A full system would include two coupled PDEs for the ligand and bound-state concentrations. However, by exploiting the high aspect ratios and large Péclet numbers associated with the device, we may reduce our system to the integrodifferential equation that results when one substitutes (13) into (5). Hence the transverse variable $z$ appears only as a parameter. Moreover, by considering the experimentally desirable case where $\mathrm{Da} \ll 1$, we may simplify the model further to obtain an ERC equation in each zone. The ERC equation includes the effective Damköhler number to account for ligand depletion due to zone geometry and placement within a column of reacting zones. We also derived bounds on Da to ensure that the system of the ERC equation remains physical. These bounds are consistent with the examined regime $\mathrm{Da} \ll 1$.

In the case of multiple reacting zones with the same receptor, we calculated both the effective Damköhler number in each zone, as well as the error made in estimating the rate constants using a naïve one-zone model. This error can be quite substantial as the row number increases.

Our model is general enough to handle a wide range of shapes for the reacting zones; the previously examined case of rectangular zones (Edwards 2011) corresponds to the case where $m \to \infty$, while the experimental case of circular zones corresponds to $m = 1$. We examined the asymptotic behavior of our expressions as $m \to \infty$, and found them to match the results from rectangular zones in the literature. Our work on circular reacting zones indicates that sensograms for $m = 1$ exhibit a minimal decrease in depletion effects compared with square reacting zone sensograms due to decreased ligand depletion.

One advantage of the Flexchip is the ability to run many interactions with different receptors simultaneously. Thus we extend our analysis to an array of reacting zones having different rate constants. Different rate constants yield zone-specific leading-order bound states, complicating the calculation of ligand depletion with time-dependent terms. We propose two methods for handling this time-dependent ligand depletion. In the first, the ERC equation is derived in the same way as in the same-receptor case, yielding additional bounds on Da so that the solution remains physical. In the second, we use a different averaging technique, which yields time-dependent $\mathrm{Da}_i$. In order to guarantee realistic results in this formulation, there are bounds on the rate constants in each column.

Unlike previous ERC equations, these must be solved numerically to produce sensograms. However, the simple nature of the ERC makes it easy to be implemented in software. With increased biosensor use, we attempt to elucidate the effect of arrays of reacting zones and suggest preferred experimental setups. With this *a priori* information for preferred array layouts and parameter regimes, biosensor users may produce and interpret better results for interaction analyses.

## References

Bhattacharyya S, Warfield KL, Ruthel G, Bavari S, Aman MJ, Hope TJ (2010) Ebola virus uses clathrin-mediated endocytosis as an entry pathway. Virology 401(1):18–28

Edwards DA (1999) Estimating rate constants in a convection-diffusion system with a boundary reaction. IMA J Appl Math 63:89–112

Edwards DA (2001) The effect of a receptor layer on the measurement of rate constants. Bull Math Biol 63:301–327

Edwards DA (2011) Transport effects on surface reaction arrays: biosensor applications. Math Biosci 230:12–22

Goldstein B, Wofsy C, Echavarría-Heras H (1988) Effect of membrane flow on the capture of receptors by coated pits. Biophys J 53:405–414

Hansen R, Bruus H, Callisen TH, Hassager O (2012) Transient convection, diffusion, and adsorption in surface-based biosensors. Langmuir 28:7557–7563

GE Healthcare (2006) Biacore flexchip product information. GE Healthcare, Uppsala

GE Healthcare (2007) Biacore AB. Label-free interaction analysis in real-time using surface plasmon resonance, Technology Note 23. GE Healthcare, Uppsala

Hu G, Gao Y, Li D (2007) Modeling micropatterned antigen-antibody binding kinetics in a microfluidic chip. Biosens Bioelectron 22:1403–1409

Mason T, Pineda AR, Wofsy C, Goldstein B (1999) Effective rate models for the analysis of transport-dependent biosensor data. Math Biosci 159:123–144

Pommier AJC, Alves G, Viennois E, Bernard S, Communal Y, Sion B, Marceau G, Damon C, Mouzat K, Caira F, Baron S, Lobaccaro JMA (2010) Liver X Receptor activation downregulates AKT survival signaling in lipid rafts and induces apoptosis of prostate cancer cells. Oncogene 29(18):2712–2723

Rich RL, Cannon MJ, Jenkins J, Pandian P, Sundaram S, Magyar R, Brockman J, Lambert J, Myszka DG (2008) Extracting kinetic rate constants from surface plasmon resonance array systems. Anal Biochem 373(1):112–120

Zumbrum M (submitted) The effect of receptor nonuniformity for surface reactions within optical biosensors. IMA J Appl Math

Zumbrum M, Edwards DA(submitted) Conformal mapping in optical biosensor applications. J Math Bio